COMPDYN 2011
III ECCOMAS Thematic Conference on
Computational Methods in Structural Dynamics and Earthquake Engineering
M. Papadrakakis, M. Fragiadakis, V. Plevris (eds.)
Corfu, Greece, 25–28 May 2011

ADAPTIVE FORCE-BASED FRAME ELEMENT FOR REGULARIZED RESPONSE

João P. Almeida[1], **Sandip Das**[1], **and Rui Pinho**[2]

[1] EUCENTRE – European Centre for Training and Research in Earthquake Engineering
Via Ferrata 1, 27100 Pavia, Italy
{joao.pacheco, sandip.das}@eucentre.it

[2] University of Pavia
Via Ferrata 1, 2700 Pavia, Italy
rui.pinho@unipv.it

Keywords: regularization; force-based; distributed plasticity; frame; numerical integration; interpolatory quadrature; Gauss-Lobatto

Abstract. *Distributed inelasticity force-based elements, widely used in earthquake engineering modeling, lose objectivity at local and global level of response in the softening range of sectional behaviour. This motivated many researchers in the past to propose various regularization techniques to trace a physically meaningful post-peak curve. However, elements that give regularized response under softening behaviour are too flexible to be used for the hardening branch.*

The present work presents a new adaptive force-based plane element that overcomes the aforementioned limitations. As the name suggests, the element is capable of providing solutions for both hardening and softening response by automatically adjusting the element integration weights when a section undergoes into softening. The latter are computed with theoretically derived closed-form expressions from interpolatory quadrature. The 'adaptive' nature of the integration scheme renders it numerically very efficient. Furthermore, the proposed element can directly account for the value of axial force installed on the element in the estimation of the corresponding length of plastification, thus creating a physically sound regularization scheme.

The performance of the proposed adaptive element is first evaluated by comparing its results with those obtained by the standard numerical integration scheme under otherwise similar conditions. It is found that for both monotonic and cyclic response the adaptive model gives good matching at a little computational effort. Moreover, the results from the current model compare well against experimental data, both in the hardening and softening ranges of behaviour.

1 INTRODUCTION

In quasibrittle materials like concrete and rock relatively large fracture zones can occur resulting from progressive growth and coalescence of microcracks, which are usually described by softening laws. Softening behaviour of constitutive law, in general, refers to the descending branch of stress with increasing strain in the stress-strain curve. In continuum mechanics, softening behaviour poses complex mathematical difficulties as the problem becomes ill-posed and the finite element (FE) results become mesh size-dependent – a phenomenon called localization. Localization precludes achieving convergence by refining the mesh size (objectivity). The present study focuses on reinforced concrete (RC) beam elements, which also exhibit similar type of numerical difficulties.

Irrespective of the type of beam formulation, force-based (FB) or displacement-based (DB), the objectivity in response is sought by adopting pre-defined characteristic mesh size within the softening zone, which is widely known as regularization. The vast majority of regularization techniques that can be found in literature for continuum finite elements – of which are particularly relevant those based on integral non-local procedures [1, 2] and gradient models [3] – are generally applied with DB FE formulations. The first proposal applicable to FB fibre-section models was based on ensuring a constant fracture energy release [4]. However, it requires a laborious member-by-member modification of the uniaxial stress-strain relationship of each fibre based on the number of integration points (IPs) and the knowledge of the compressive fracture energy, which may not be easily available. Further, the global force-displacement response needs to be post-processed, using the physical characteristic length, to warrant an objective prediction of the curvature demand in the localized damage zone. On the other hand, the more straightforward regularization proposals by Scott and Fenves [5] and Addessi and Ciampi [6] are likely to produce too flexible solutions for the simulation of the hardening phase of behaviour.

Scott and Hamutçuoglu [7] recently proposed a numerically consistent regularization method that is able to accurately model both hardening and softening ranges of sectional behaviour. This is achieved by adding two additional IPs very close to the element ends, their weights being selected to ensure convergence for both types of sectional behaviours. However, the order of accuracy of their scheme is only of $N - 5$, N being the total number of IPs (including those close to the extremities), which means that for the solution of linear-elastic frame elements at least seven IPs should always be used. Additionally, the element performance is highly sensitive to the position of the two extra IPs.

The present study proposes a novel beam element featuring an adaptive integration method that has the ability of continuously controlling the IP weights, while preserving their positions, in order to maximize accuracy for strain-hardening sectional behaviour and maintain objectivity for strain-softening response. The central idea of the formulation is presented and several numerical verification examples are shown along with pertinent discussion.

2 PROPOSED REGULARIZATION TECHNIQUE

In FB elements, in order to control the beam end sections subjected to larger bending moments, Gauss-Lobatto (GL) quadrature (that includes IPs in the extremities of the integration interval) is commonly used. It has a high order of accuracy of degree $2N - 3$, where N is the number of IPs. On the other hand, the typical regularized integration schemes, restrained by the imposition of some pre-defined weights, have less order of accuracy.

The main idea of the present proposal is to allow the commutation, automatically during the loading history, between different numerical integration schemes in order to ensure high accuracy during hardening and also objective solution during softening response.

In order to monitor the history of section forces and deformations during the analysis, IP positions should not be varied and, consequently, only the corresponding weights are adaptively adjusted. Additionally, in order to pass a patch test, the element has to provide at least the linear-elastic solution; i.e. 2nd degree polynomials need to be integrated exactly.

In the present study, the IP positions considered are same as those of the GL integration scheme. Consequently, throughout the hardening branches, the weights of the several IPs are also defined as those of the standard GL quadrature. The full hardening case is denoted as case (a), for future reference. Whenever a section is softening, the associated integration weight of that section is adjusted to match the appropriate normalized characteristic length. Further, it is assumed that softening can only occur in one or both extremity sections. Once the element starts to soften, the integration weights of the several IPs are recomputed under the condition that the extreme integration weights match λ_{pI} or/and λ_{pJ} (respectively the normalized characteristic lengths of the initial and final sections). In the earthquake engineering modelling context, the characteristic length of a certain IP, L_p, can be assumed to be equal to the plastic hinge length (this term is adopted in the current manuscript, although the correct expression would be 'length of plastification'). The corresponding integration weight λ_p (i.e. the normalized characteristic length) can thus be computed as $(b - a)\ L_p / L_0$, where L_0 is the length of the element. In case of softening, one of the following three cases is bound to happen (typically, cases (b) or (c) will occur first, then (d) will follow for larger inelastic demands):

- Case (b): Softening of the initial IP. In this case, the integration weight of the initial IP matches the normalized characteristic length λ_{pI} ($w_1^* = \lambda_{pI}$). The computation of the integration weights of the remaining IPs can be achieved through interpolatory quadrature [8, 9], the goal of which is to select the weights $w_2^*, w_3^*, ..., w_N^*$ such that the error

$$E(f) = \int_a^b f(x)\,dx - \sum_{j=1}^{N} w_j^* f(x_j) \underset{w_1^*=\lambda_{pI}}{=} \int_a^b f(x)\,dx - \lambda_{pI} f(x_1) - \sum_{j=2}^{N} w_j^* f(x_j) \tag{1}$$

  is zero for $f(x) = 1, x, ..., x^{N-2}$. It is noted that a general integration interval $[a,b]$ was used. Considering the positions of the GL integration scheme, the following linear system of $N-1$ equations and $N-1$ unknown weights $w_2^*, w_3^*, ..., w_N^*$ is obtained:

$$\begin{aligned}
&\lambda_{pI} + w_2^* + w_3^* + ... + w_N^* = \int_a^b dx \\
&\lambda_{pI} a + w_2^* x_2 + w_3^* x_3 + ... + w_N^* b = \int_a^b x\,dx \\
&\vdots \\
&\lambda_{pI} a^{N-2} + w_2^* x_2^{N-2} + w_3^* x_3^{N-2} + ... + w_N^* b^{N-2} = \int_a^b x^{N-2}\,dx
\end{aligned} \tag{2}$$

  or, equivalently:

$$\begin{bmatrix} 1 & 1 & \dots & 1 \\ x_2 & x_3 & \dots & b \\ \vdots & \vdots & & \vdots \\ x_2^{N-2} & x_3^{N-2} & \dots & b^{N-2} \end{bmatrix} \begin{bmatrix} w_2^* \\ w_3^* \\ \vdots \\ w_N^* \end{bmatrix} = \begin{bmatrix} b-a-\lambda_{pI} \\ \left(b^2-a^2\right)/2-\lambda_{pI}a \\ \vdots \\ \left(b^{N-1}-a^{N-1}\right)/(N-1)-\lambda_{pI}a^{N-2} \end{bmatrix} \tag{3}$$

- Case (c): Softening of the final IP. In this case, the integration weight of the final IP matches the normalized characteristic length λ_{pJ} ($w_N^{**} = \lambda_{pJ}$). An analogous rationale to case (b) can be applied and the unknown weights $w_1^{**}, w_2^{**}, ..., w_{N-1}^{**}$ obtained through the next system of equations:

$$\begin{bmatrix} 1 & 1 & \dots & 1 \\ a & x_2 & \dots & x_{N-1} \\ \vdots & \vdots & & \vdots \\ a^{N-2} & x_2^{N-2} & \dots & x_{N-1}^{N-2} \end{bmatrix} \begin{bmatrix} w_1^{**} \\ w_2^{**} \\ \vdots \\ w_{N-1}^{**} \end{bmatrix} = \begin{bmatrix} b-a-\lambda_{pJ} \\ \left(b^2-a^2\right)/2-\lambda_{pJ}b \\ \vdots \\ \left(b^{N-1}-a^{N-1}\right)/(N-1)-\lambda_{pJ}b^{N-2} \end{bmatrix} \tag{4}$$

- Case (d): Softening of both end IPs. The numerical weights of the initial and final end IPs should match λ_{pI} and λ_{pJ} ($w_1^{***} = \lambda_{pI}$ and $w_N^{***} = \lambda_{pJ}$) respectively. Again, interpolatory quadrature can be used to compute the intermediate integration weights:

$$\begin{bmatrix} 1 & 1 & \dots & 1 \\ x_2 & x_3 & \cdots & x_{N-1} \\ \vdots & \vdots & & \vdots \\ x_2^{N-3} & x_3^{N-3} & x_4^{N-3} & x_5^{N-3} \end{bmatrix} \begin{bmatrix} w_2^{***} \\ w_3^{***} \\ \vdots \\ w_{N-1}^{***} \end{bmatrix} = \begin{bmatrix} b-a-\lambda_{pI}-\lambda_{pJ} \\ \left(b^2-a^2\right)/2-a\lambda_{pI}-b\lambda_{pJ} \\ \vdots \\ \left(b^{N-2}-a^{N-2}\right)/(N-2)-a^{N-3}\lambda_{pI}-b^{N-3}\lambda_{pJ} \end{bmatrix} \tag{5}$$

The order of accuracy for cases (b) and (c) is of $N-2$, while for case (d) is of $N-3$. This implies that the minimum number of integration points to be used in the present adaptive element is five, which matches the approximate minimum number of IPs for objective strain-hardening response. It is recalled that the integration weights are used for the numerical integration required to compute the vector of basic displacements and the tangent flexibility matrix of the element.

The calculation of the IP weights for cases (b), (c) and (d) has to be performed continuously throughout the softening branch(es) if the characteristic length depends on the sectional force. This is however an inexpensive operation from the numerical viewpoint, since closed-form solutions can be easily derived. For example, the closed-form solution for 5 IPs and cases (b), (c) and (d) (taking $a=-1$ and $b=1$) is, respectively:

$$\begin{bmatrix} w_2^* \\ w_3^* \\ w_4^* \\ w_5^* \end{bmatrix} = \begin{bmatrix} \frac{7}{9} - \frac{7}{3}\lambda_{pI} \\ \frac{4}{9} + \frac{8}{3}\lambda_{pI} \\ \frac{7}{9} - \frac{7}{3}\lambda_{pI} \\ \lambda_{pI} \end{bmatrix}, \quad \begin{bmatrix} w_1^{**} \\ w_2^{**} \\ w_3^{**} \\ w_4^{**} \end{bmatrix} = \begin{bmatrix} \lambda_{pJ} \\ \frac{7}{9} - \frac{7}{3}\lambda_{pJ} \\ \frac{4}{9} + \frac{8}{3}\lambda_{pJ} \\ \frac{7}{9} - \frac{7}{3}\lambda_{pJ} \end{bmatrix}, \quad \begin{bmatrix} w_2^{***} \\ w_3^{***} \\ w_4^{***} \end{bmatrix} = \begin{bmatrix} \frac{7}{9} - \frac{\sqrt{21}}{6}\left(\lambda_{pI} - \lambda_{pJ}\right) - \frac{7}{6}\left(\lambda_{pI} + \lambda_{pJ}\right) \\ \frac{4}{3}\left(\frac{1}{3} + \lambda_{pI} + \lambda_{pJ}\right) \\ \frac{7}{9} + \frac{\sqrt{21}}{6}\left(\lambda_{pI} - \lambda_{pJ}\right) - \frac{7}{6}\left(\lambda_{pI} + \lambda_{pJ}\right) \end{bmatrix} \quad (6)$$

Figure 1 schematically describes the representation of a computed distribution of integration weights for the previous cases, considering arbitrary values of λ_{pI} and λ_{pJ}. It should be mentioned that the success of the current adaptive element is dependent on the correct identification of the sectional behaviour (hardening or softening). The description of the technique developed for such purpose, and implemented in an *ad hoc* computer code, as well as the associated state determination algorithm, falls out of the scope of this document. Nevertheless, the interested reader can find it in Almeida *et al.* [10]. Finally, it is noted that linear geometry is assumed.

3 NUMERICAL EXAMPLES

3.1 Laterally loaded cantilever

The performance of the proposed adaptive element is first demonstrated with the help of an idealized multi-linear moment-curvature relationship with initial post-yield hardening followed by a softening branch. Figure 2 shows the normalized moment-curvature relationship, where moment and curvatures are normalized by the ultimate moment (M_u) and the corresponding curvature (χ_u) respectively. Elastic unloading behaviour is considered. Furthermore, it is assumed that the softening branch will continue with the same slope for a higher demand of normalized curvature beyond two.

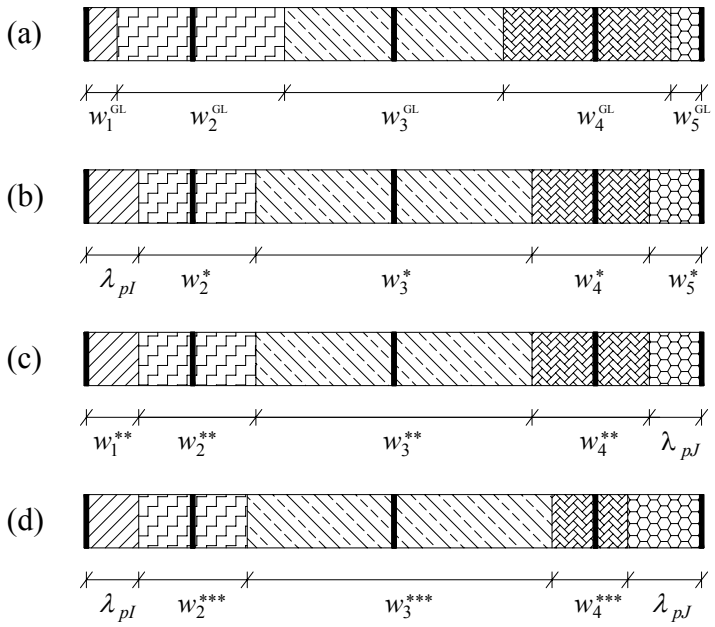

Figure 1: Illustrative example of weight computation: (a) Gauss-Lobatto; (b) softening of initial section; (c) softening of final section; (d) softening of both end sections.

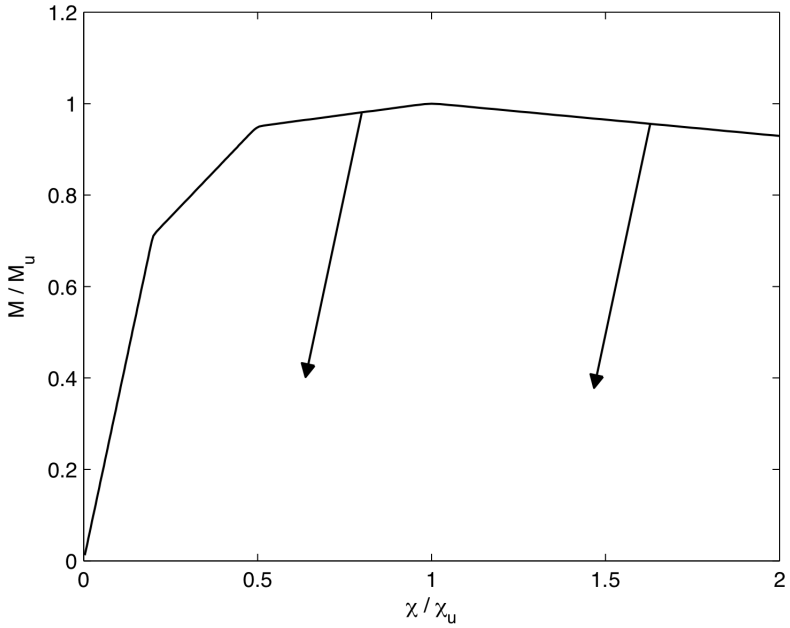

Figure 2: Idealized normalized multi-linear moment-curvature relationship.

Figure 3 shows the top lateral force, normalized by its ultimate value, versus top lateral drift (Δ) ratio of a cantilever column (modelled by a single element). Results for standard GL and for the new adaptive integration schemes with different numbers of IPs are compared. The characteristic length L_p is arbitrarily assumed to be $0.15L$, where L is the shear span associated to the bottom critical section (in the present case it corresponds to the full element length L_0).

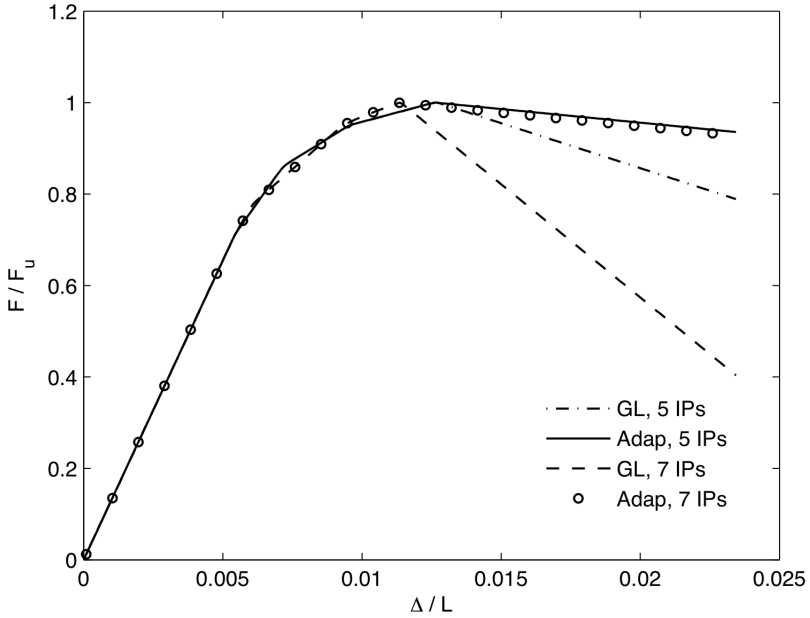

Figure 3: Normalized top lateral force versus top lateral drift ratio of the cantilever column in the cases of standard GL and adaptive schemes, for different number of IPs.

It can be observed, as expected, that during the hardening phase of response the new adaptive and the standard GL schemes yield identical results for the same number of IPs because there is a continuous correspondence between the integration weights employed. The difference in responses during the hardening phase is due to the number of IP-dependent spreading of inelasticity within the element, which is however objective. This is also the reason why the peak lateral loads correspond to different values of lateral drift for five and seven IPs. However, for the softening branch, a clear non-objective response is apparent for the standard GL scheme with different number of IPs, while the adaptive scheme produces an objective output.

Figure 4 shows the distribution of curvature at the end of the loading phase along the normalized length of the element. It is clear from the figure that for standard GL scheme the curvature demand at the initial section increases with increasing number of IPs because, during the softening branch, spreading of inelasticity is not possible. However, for the adaptive scheme the curvature demand is objective because it uses regularized integration weight for the initial section.

The ability of the adaptive element to switch the integration weights from those of standard GL to those of interpolatory quadrature, by identifying the type of sectional behaviour, is shown in Figure 5. The variations of the weights for the initial section during the entire loading history and different numbers of IPs are shown for this purpose. It should be noted that the sum of all IP weights adds up to 2, i.e. in equation (1) it is assumed $a = -1$ and $b = 1$.

The previous numerical cases show the results when the column is loaded monotonically. It will also be interesting to see the behaviour under cyclic loading since this will imply a cyclic commutation between the integration weights of standard GL and interpolatory quadrature. Figure 6 shows the general cyclic behaviour of the multi-linear moment-curvature relationship, which has the same monotonic behaviour as that of Figure 2.

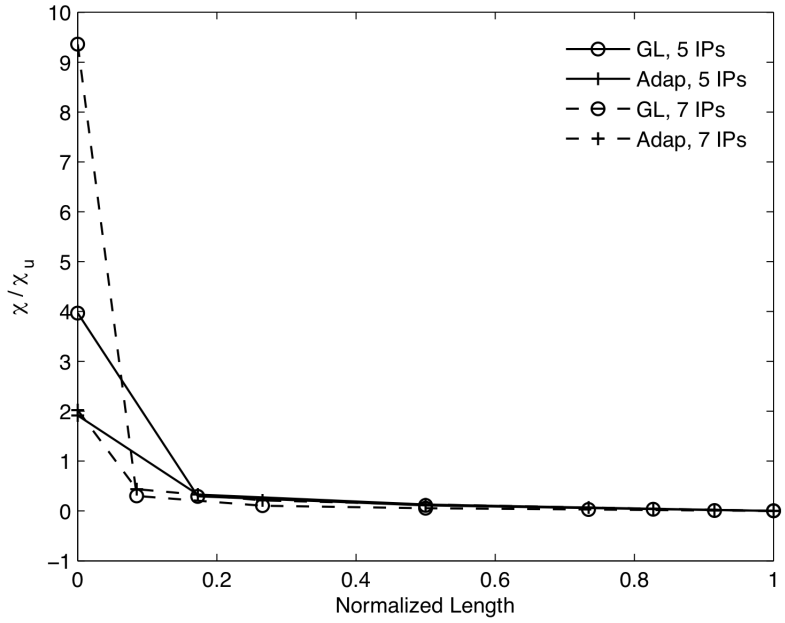

Figure 4: Normalized curvatures at the end of loading phase along the normalized length of the element, in the cases of GL and adaptive schemes for different number of IPs.

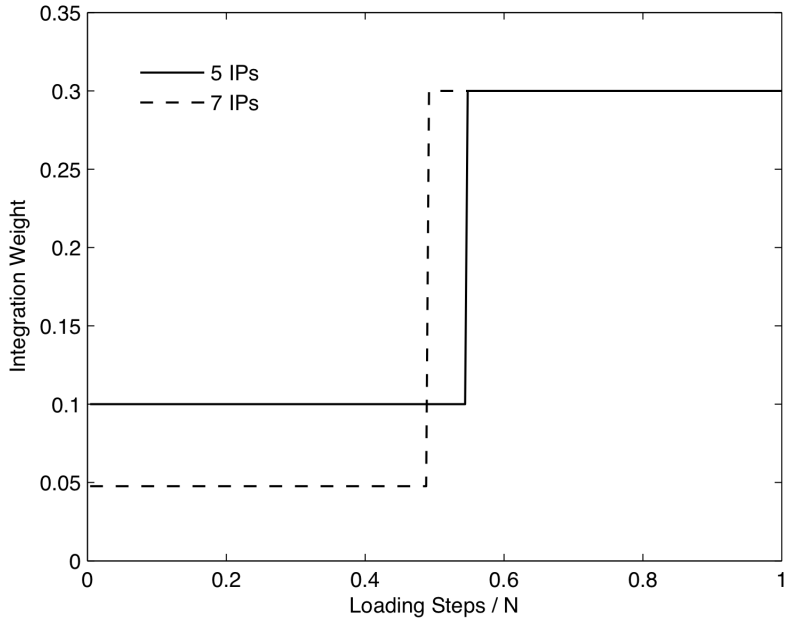

Figure 5: Variation of integration weight at the initial IP along normalized loading steps (N = total number of loading steps) in the case of adaptive element with different IPs.

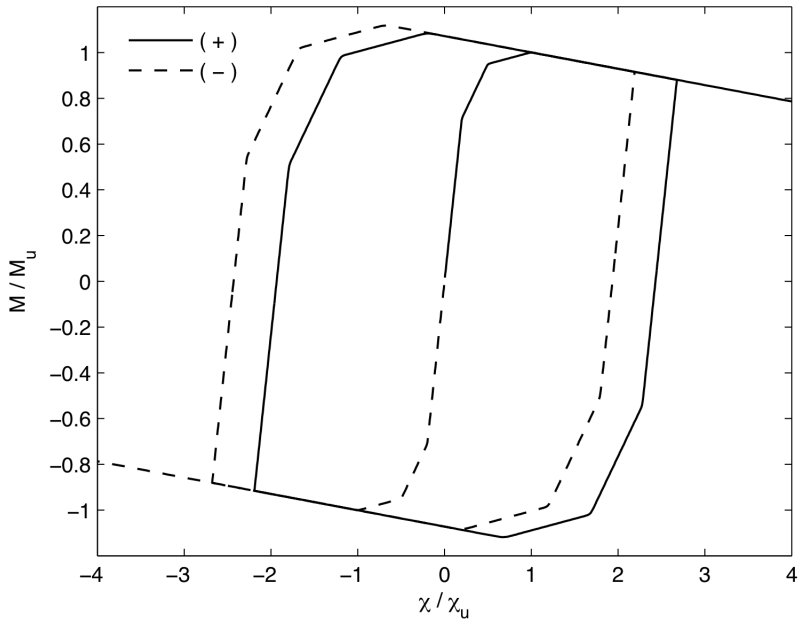

Figure 6: Multi-linear cyclic moment-curvature rule for positive and negative initial elastic loadings.

Figure 7 depicts the normalized top lateral force versus top lateral drift ratio for different integration schemes, with five and seven IPs, under cyclic loading. The entire loading phase has three salient parts chronologically, viz., the loading phase (increasing drift ratio), the unloading phase (decreasing drift ratio) and the reloading phase (again increasing drift ratio). At the end of the loading phase the results are identical to the previous monotonic case. When the unloading starts, the sectional response becomes of the hardening type and thus the integration weights for the adaptive scheme change back to those of the standard GL. At the initiation of softening towards the end of the unloading phase they again commute to those of

the interpolatory quadrature, and so on. Consequently, the adaptive scheme yields an objective response for the entire cyclic load history. The commutation of integration weights for the initial section is shown in Figure 8. One thing to be noticed in Figure 7 is that the softening for standard GL with seven IPs is less pronounced in the unloading phase and also the final force level is much lower. This is due to the shift of localization from the extremity section to the adjacent one, a phenomenon that can happen during cyclic behaviour for elements with large number of IPs, and that was observed and explained by Almeida *et al.* [10].

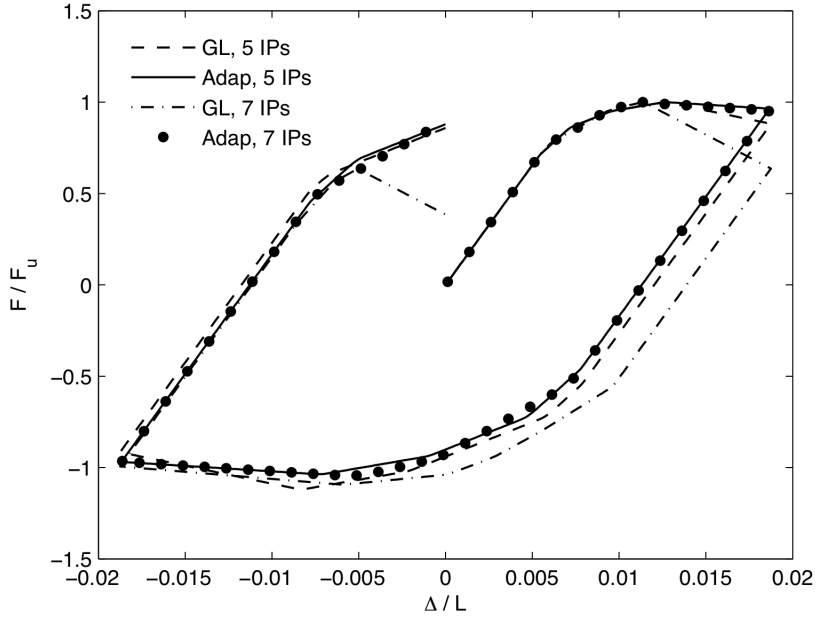

Figure 7: Normalized top lateral force versus top lateral drift ratio for adaptive and standard GL schemes with five and seven IPs.

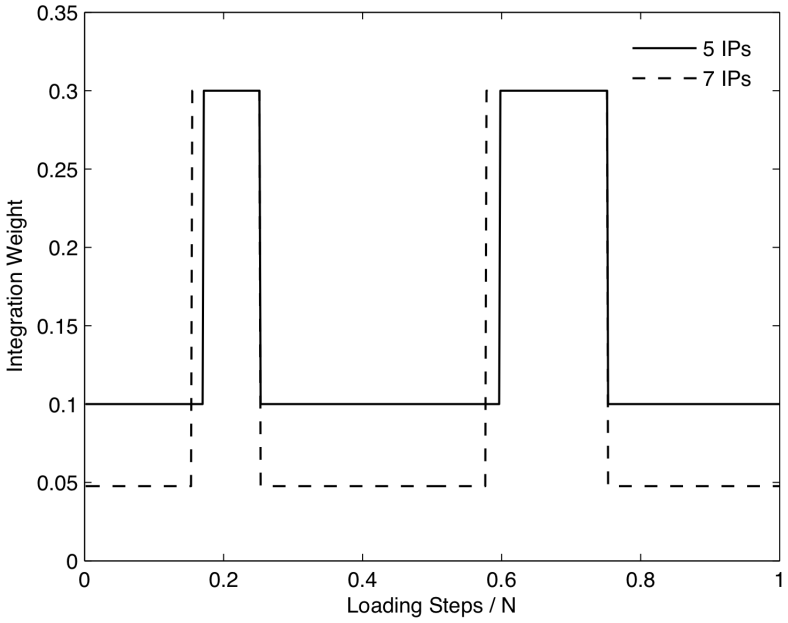

Figure 8: Variation of integration weights for the initial section during the entire load history in the cases of adaptive element with five and seven IPs.

The effects of such shift can be observed in Figure 9, which shows the curvature distributions along the normalized length of the element at the end of the cyclic loading phase. It is apparent that for GL with 7 IPs, unlike for the 5-IPs' GL case, there is a curvature reversal throughout the element length, which is attributable to the previous numerical occurrence.

3.2 Columns subjected to varying axial loads

The adaptive scheme's ability to continuously adjust the characteristic length can be best utilized by considering response-dependent characteristic length. This feature can be of relevance in real applications, e.g. columns located at the boundary of frame structures subjected to earthquake loading, where the axial load (due to global overturning moment) is expected to fluctuate. For this case-study, two cantilever columns of length L, viz. Column 1 and Column 2, are modelled by one element. A maximum lateral displacement (Δ) of $0.04L$ (4% drift) is imposed, as well as two different axial load ratios that vary during lateral displacement according to Figure 10. The axial load ratio, ρ_A, is defined as the ratio of the axial load to the ultimate axial load capacity of the section. From the figure it is clear that the gravity load and the maximum plus/minus variation correspond to ρ_A of 0.25.

The monotonic moment-curvature relationship with origin-oriented linear unloading, as shown in Figure 11, is adopted for the present case. An elastic constitutive law is assumed for the axial behaviour, which is uncoupled from the flexural response.

Since the characteristic length can depend on the level of axial force (e.g., [11]), a purely illustrative law is considered for the characteristic length. It is a function of ρ_A as:

$$L_p / L = \max[0.5\rho_A, 0.15] \tag{7}$$

where max[.] indicates the maximum of the two arguments.

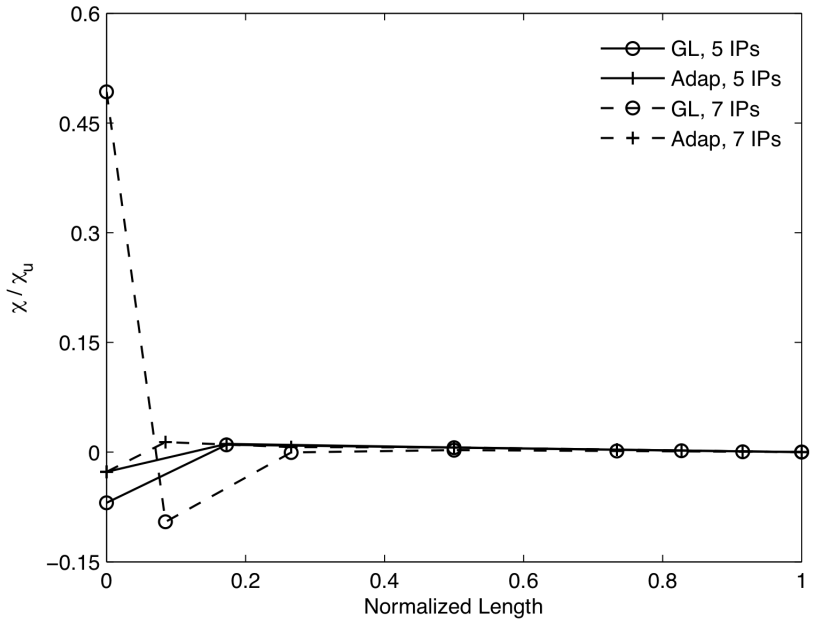

Figure 9: Normalized curvatures at the end of cyclic loading phase along the normalized length of the element, in the cases of GL and adaptive schemes for different number of IPs

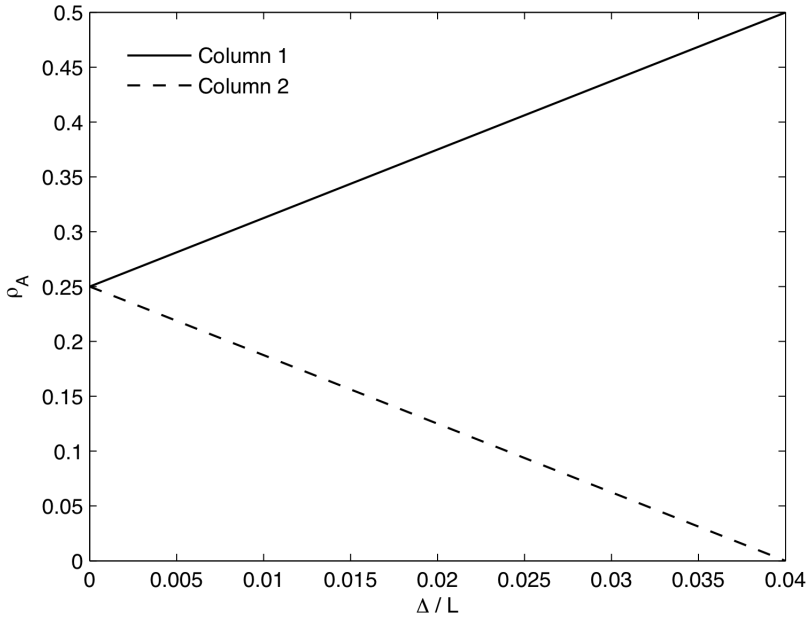

Figure 10: Variation of axial load ratio in Columns 1 and 2 with lateral drift.

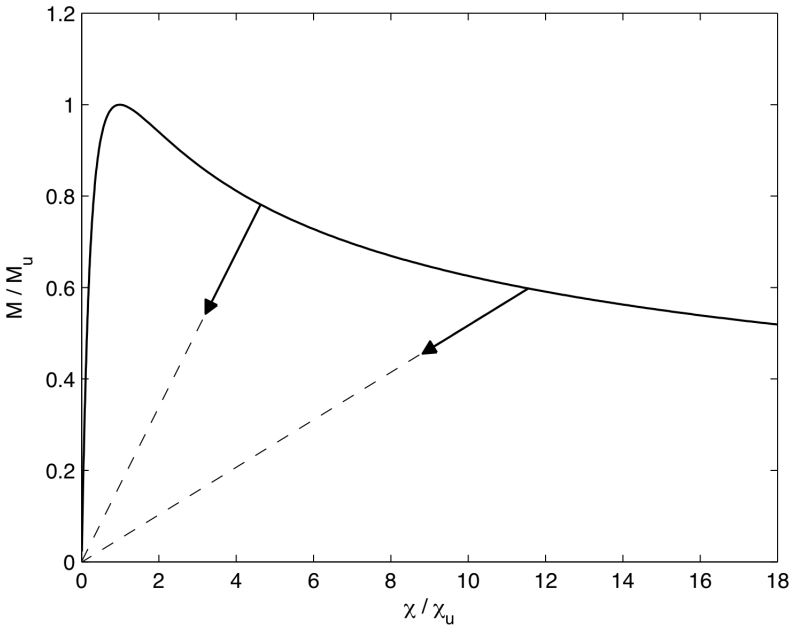

Figure 11: Idealized moment-curvature relationship.

The responses of Column 1 and Column 2 for standard GL and adaptive integration schemes with five and seven IPs are shown in Figure 12. It can be noticed that, once again, the present adaptive element provides objective response for each column and different number of IPs. The difference between both columns depicts obviously the influence of the varying axial force in the computation of the applicable characteristic length, as given by equation (7). Figure 13 shows the evolution of the initial integration weight, for the case of 5 IPs, remaining clear that for Column 2 it is less than for Column 1, due to the lower axial load ratio. It should be mentioned that the integration weight for Column 2 during softening is governed

by the minimum criterion of $L_p = 0.15L$. On the other hand, the integration weight for Column 1 increases in proportion to the increasing axial load. The behaviour of the element with non-regularized GL scheme shows (see Figure 12) not only the typical localization phenomena associated to distinct number of IPs but also the expected insensitivity to the varying values of the axial force.

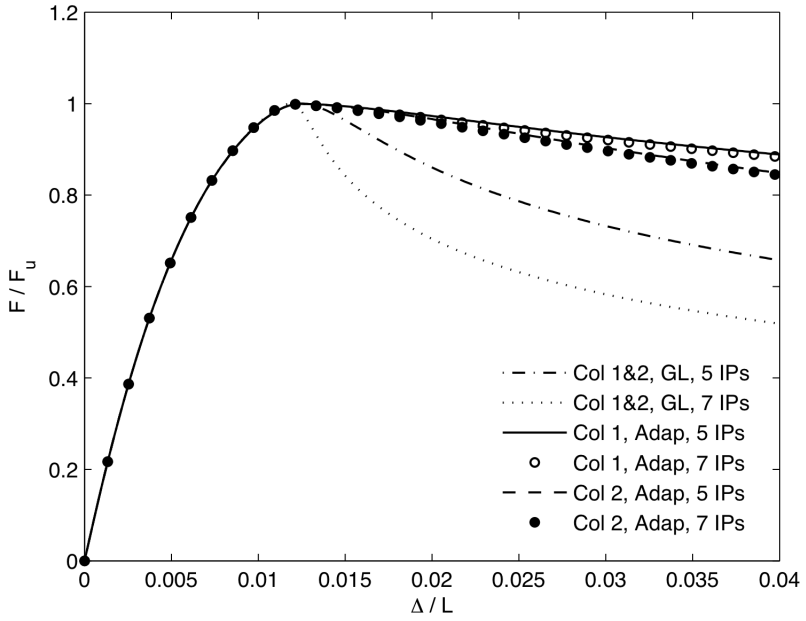

Figure 12: Responses of Column 1 and Column 2 at different levels of drift, for GL and adaptive integration schemes with different number of IPs.

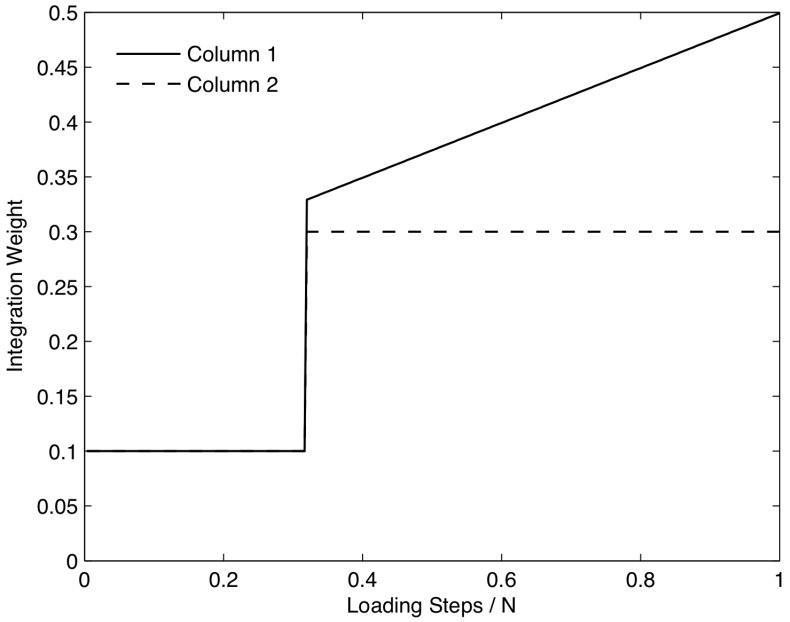

Figure 13: Variation of integration weight at initial IP for adaptive element with five IPs.

3.3 Experimentally tested column

The previous numerical examples intend to highlight the theoretical aspects of the proposed adaptive numerical scheme. Its application to model reinforced concrete member behaviour is now briefly addressed.

The test specimen U-5 of Watson and Park [12] has been used for experimental verification. The equivalent cantilever length of the column specimen is 1.6 m, where the cross section is 400 by 400 mm. The uniaxial concrete properties are f_{c0} = 41 MPa, f_{cc} = 53.3 MPa, ε_{c0} = 0.0027 and ε_{cc} = 0.00675 and the yield stress for longitudinal steel is 474 MPa. The column is subjected to a constant axial force of 3280 kN (axial load ratio of 0.5).

The cantilever is modelled by a single FB element and the sectional response is given by a classical concrete/steel fibre discretization approach. The uniaxial laws considered for concrete and steel are due to Martinez-Rueda and Elnashai [13] and Menegotto and Pinto [14] respectively. For concrete in traction an exponential decay was used to account for tension-stiffening effects. Moreover, two different formulae for plastic hinge length, representative of the characteristic length, due to Paulay and Priestley [15] and Bae and Bayrak [11] have been considered.

Figure 14 shows the monotonic envelopes predicted by the standard GL scheme with five and seven IPs, by the adaptive scheme with five IPs and different formulae for the plastic hinge length, as well as the experimental cyclic curves. The lateral force that equates the moment due to P-Δ effect is added to the experimentally applied horizontal force at each step for comparison with numerical results. It is clear from the figure that the adaptive schemes predict the monotonic backbone curve quite accurately while those predicted by the standard GL scheme are not acceptable (in the softening range). It is recalled that in the case of standard GL scheme, a steeper softening slope is due to an unrealistic concentration of curvature demand at the base for a specified lateral displacement at the column top.

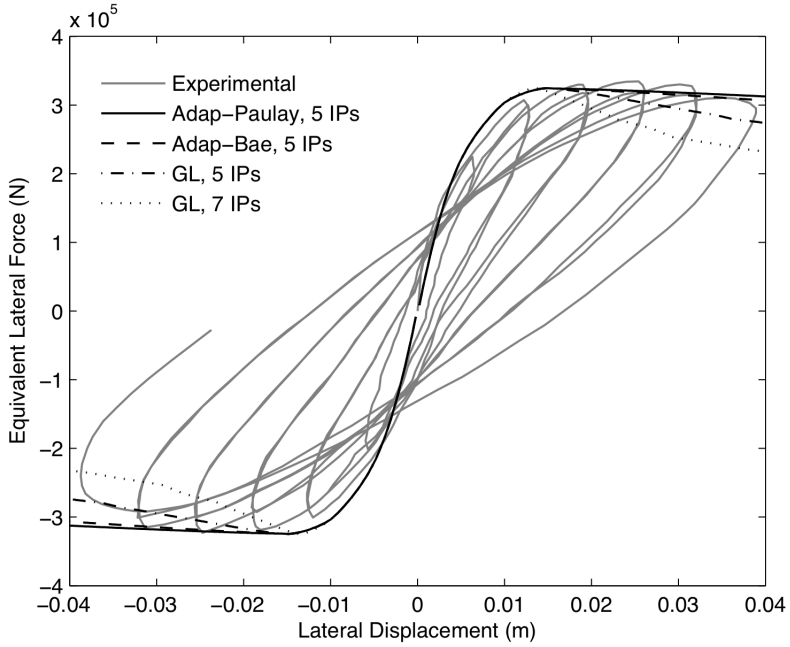

Figure 14: Comparison of experimental (cyclic) and numerical (monotonic) curves in the cases of standard GL and adaptive scheme (with different formulae of plastic hinge length), for different number of IPs.

The values of curvature demand along the length for the different cases are shown in Figure 15. For the GL scheme with five and seven IPs the curvature is unrealistically high (respectively around three and six times the objective value provided by the adaptive scheme). Figure 16 shows the moment-curvature demands for the adaptive scheme (with Bae and Bayrak's formula for plastic hinge length) and the standard GL scheme, with five IPs. Only the results corresponding to regular increments of the top node lateral displacement are depicted. As expected, it can be seen that the demands are identical up to the onset of softening, after which the rate of curvature increase is higher for the GL scheme than for the adaptive one.

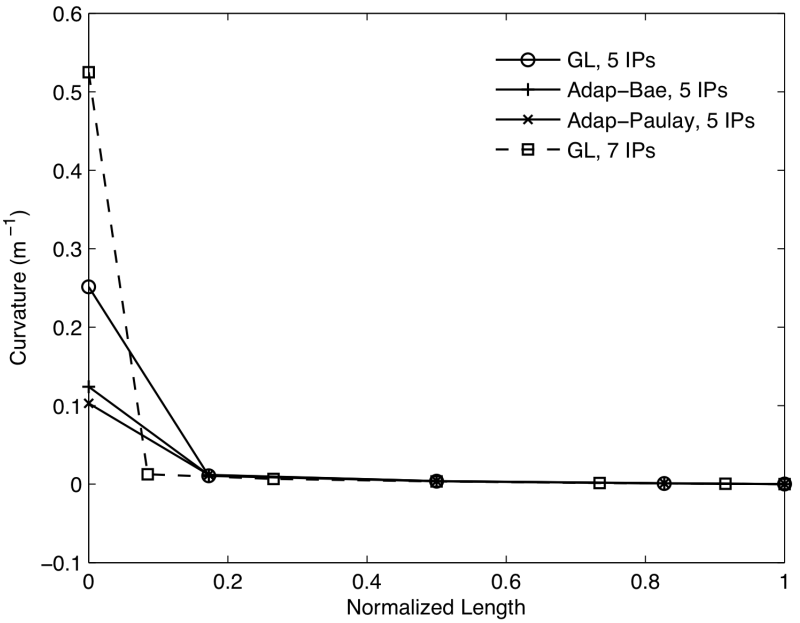

Figure 15: Curvature distribution along the normalized column length at the end of the loading phase, in the cases of standard GL and adaptive scheme (with different formulae of plastic hinge length).

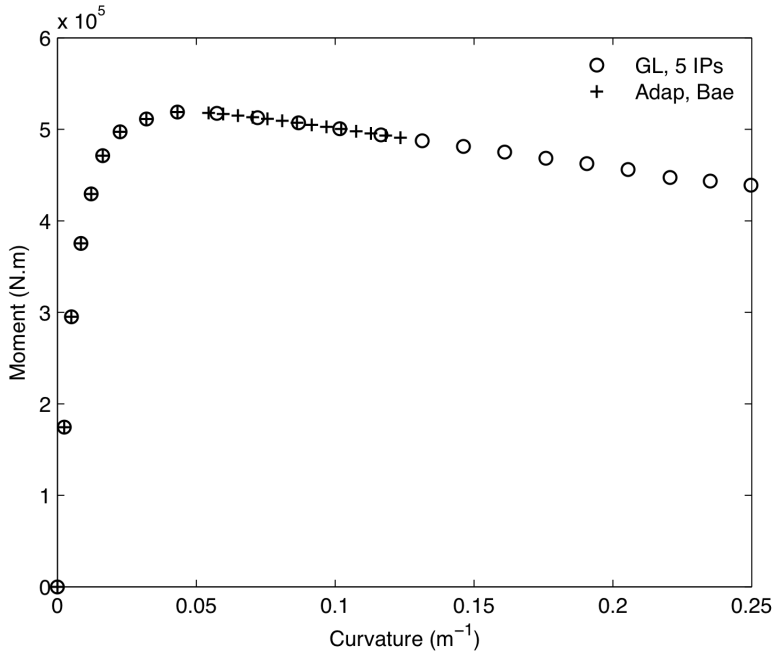

Figure 16: Comparison of monotonic curvature demands for Watson and Park's test specimen in the cases of standard GL and adaptive scheme (using Bae and Bayrak's formula for plastic hinge length) with 5 IPs.

4 CONCLUSIONS

A new load adaptive FB frame element was proposed, the integration scheme of which can automatically commute between the integration weights of standard GL and characteristic length-based interpolatory quadrature, depending on the type of sectional behavior (hardening or softening). This enables the element's integration scheme to maintain the high order of accuracy of the standard GL scheme during the hardening phase(s), while guaranteeing objective response during the softening part(s) of the response.

A number of numerical applications have been carried out to show the different features of the newly developed adaptive element and to emphasize its advantages over the standard GL integration scheme. It has been found that, although being computationally light, the proposed element can produce objective responses for distinct number of IPs. Additionally, this regularization technique also accounts directly for the axial load variation during softening response – an aspect that cannot be addressed by the currently existing regularization methods, based on pre-defined integration schemes. Finally, the current proposal was also verified against an experimental test, where it proved to yield accurate and realistic results.

REFERENCES

[1] G. Pijaudier-Cabot, Z.P. Bazant, Nonlocal damage theory. *Journal of Engineering Mechanics* (ASCE), **113**, 1512-1533, 1987.

[2] M. Jirásek, S. Rolshoven, Comparison of integral-type nonlocal plasticity models for strain-softening materials. *International Journal of Engineering Science*, **41**, 1553-1602, 2003.

[3] R.H.J. Peerlings, M.G.D. Geers, R. de Borst, W.A.M. Brekelmans, A critical comparison of nonlocal and gradient-enhanced softening continua. *International Journal of Solids and Structures*, **38**, 7723-7746, 2001.

[4] J. Coleman, E. Spacone, Localization issues in force-based frame elements. *Journal of Structural Engineering* (ASCE), **127**, 1257-1265, 2001.

[5] M.H. Scott, G.L. Fenves, Plastic hinge integration methods for force-based beam-column elements. *Journal of Structural Engineering* (ASCE), **132**, 244-252, 2006.

[6] D. Addessi, V. Ciampi, A regularized force-based beam element with a damage-plastic section constitutive law. *International Journal for Numerical Methods in Engineering*, **70**, 610-629, 2007.

[7] M.H. Scott, O.M. Hamutçuoglu, Numerically consistent regularization of force-based frame elements. *International Journal for Numerical Methods in Engineering*, **76**, 1612-1631, 2008.

[8] P.J. Davis, P. Rabinowitz, *Methods of numerical integration, 2nd Edition*. Dover Publications, 1975.

[9] P.K. Kythe, M.R. Schaferkotter, *Handbook of computational methods for integration*. CRC Press, 2004

[10] J.P. Almeida, S. Das, R. Pinho, Adaptive force-based frame element for regularized monotonic and cyclic response. *Computers and Structures* (under review).

[11] S. Bae, O. Bayrak, Plastic hinge length of reinforced concrete columns. *ACI Structural Journal*, **105**, 290-300, 2008.

[12] S. Watson, R. Park, Design of reinforced concrete frames of limited ductility. *Report 89-4*, *Department of Civil Engineering, University of Canterbury, Christ Church, New Zealand*, 1989.

[13] J.E. Martinez-Rueda, A.S. Elnashai, Confined concrete model under cyclic load. *Materials and Structures*, **30**, 139-147, 1997.

[14] M. Menegotto, P.E. Pinto, Method of analysis of cyclically loaded RC plane frames including changes in geometry and non-elastic behaviour of elements under normal force and bending. *Preliminary Report, IABSE*, **13**, 15-22, 1973.

[15] T. Paulay, M.J.N. Priestley, *Seismic design of reinforced concrete and masonry buildings*. John Wiley and Sons, 1992.